


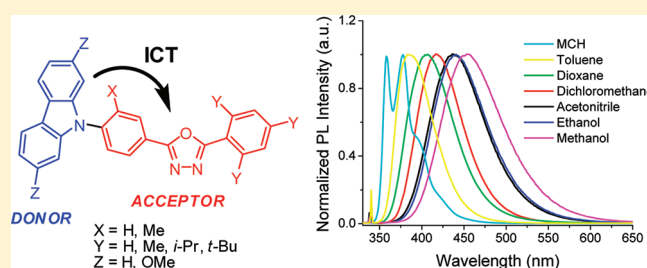
# Bipolar Molecules with High Triplet Energies: Synthesis, Photophysical, and Structural Properties

Yonghao Zheng,<sup>†</sup> Andrei S. Batsanov,<sup>†</sup> Vyngintas Jankus,<sup>‡</sup> Fernando B. Dias,<sup>‡</sup> Martin R. Bryce,<sup>\*,†</sup> and Andrew P. Monkman<sup>\*,‡</sup>

<sup>†</sup>Department of Chemistry and <sup>‡</sup>Department of Physics, Durham University, Durham, DH1 3LE, U.K.

 Supporting Information

**ABSTRACT:** This article sheds new light on the interplay of electronic and conformational effects in luminescent bipolar molecules. A series of carbazole/1,3,4-oxadiazole hybrid molecules is described in which the optoelectronic properties are systematically varied by substituent effects which tune the intramolecular torsion angles. The synthesis, photophysical properties, cyclic voltammetric data, X-ray crystal structures, and DFT calculations are presented. Excited state intramolecular charge transfer (ICT) is observed from the donor carbazole/2,7-dimethoxycarbazole to the acceptor phenyl/diphenyloxadiazole moieties. Introducing more bulky substituents onto the diphenyloxadiazole fragment systematically increases the singlet and triplet energy levels ( $E_S$  and  $E_T$ ) and blue shifts the absorption and emission bands. The triplet excited state is located mostly on the oxadiazole unit. The introduction of 2,7-dimethoxy substituents onto the carbazole moiety lowers the value of  $E_S$ , although  $E_T$  is unaffected, which means that the singlet–triplet gap is reduced (for **7b**  $E_S - E_T = 0.61$  eV). A strategy has been established for achieving unusually high triplet levels for bipolar molecules ( $E_T = 2.64$ – $2.78$  eV at 14 K) while at the same time limiting the increase in the singlet energy.



## INTRODUCTION

Controlling exciton migration in functional  $\pi$ -systems<sup>1–5</sup> is a central concept in the emerging technologies of molecular electronics<sup>6,7</sup> and optoelectronic devices,<sup>8,9</sup> including photovoltaic cells<sup>10</sup> and organic light-emitting diodes (OLEDs).<sup>11–14</sup> Numerous families of molecules<sup>15,16</sup> have been studied with the aims of optimizing  $\pi$ -conjugation, the energies of singlet and triplet excited states, energy transfer processes, and subsequent decay pathways. For example, interchromophore separation,<sup>17</sup> *meta* versus *para* phenyl substitution,<sup>18–21</sup> and molecular twisting controlled by steric effects<sup>22–24</sup> have all been exploited to chemically tailor the optoelectronic properties of conjugated  $\pi$ -systems.

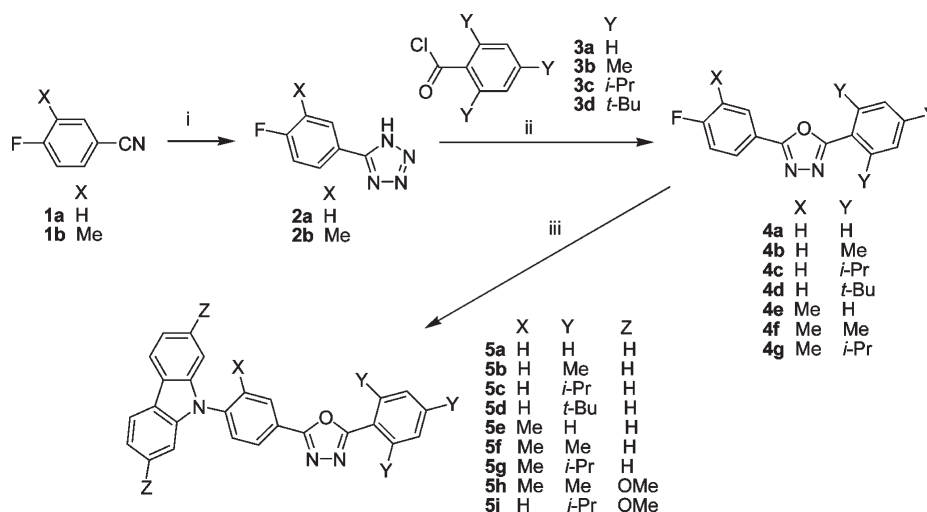
Bipolar molecules, which can accept and transport both holes and electrons, are attractive candidates for optoelectronic studies.<sup>25–34</sup> Molecules with comparable hole- and electron-transporting abilities are also called ambipolar materials.<sup>27,34</sup> In the OLED field, a major drawback of bipolar materials as hosts for guest emitters is the compression of the HOMO–LUMO gap due to intramolecular charge transfer (ICT) between the electron-donating (D) and the electron-accepting (A) moieties. This results in lowering of the singlet and triplet energies<sup>35</sup> which, in turn, leads to back-transfer of energy from the guest to the host, thereby reducing the device efficiency. It is a significant challenge, therefore, to obtain a high triplet energy state in a bipolar D–A system. Of perhaps greater importance to OLED materials is an ability to create molecules with a high triplet energy while at the same time keeping the HOMO–LUMO gap

at a level which affords easy injection of both electrons and holes into a layer of the material or at least gives easy injection of one charge and good blocking of the opposite charge. An important goal here would be to independently achieve tuning of the triplet and singlet levels of a molecule. Only in such cases can the bipolar hosts be utilized in high efficiency devices. Thus, there are very strict parameters which govern the design of a potentially useful bipolar host material.

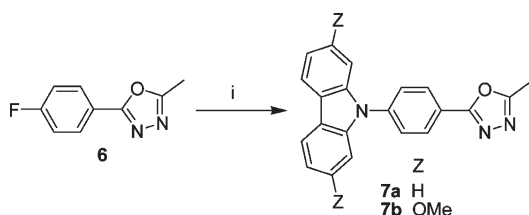
To address this issue, we chose carbazole (Cz) as the electron donor moiety. Cz is a popular component of optoelectronic materials;<sup>36,37</sup> it is easy to functionalize, is thermally very stable, has a high triplet energy (3 eV),<sup>38</sup> and has good hole-transporting ability. For example, 4,4'-*N,N'*-dicarbazolylbiphenyl (CBP) is a conventional host material for phosphorescent emitters.<sup>39–42</sup> The shortcomings of CBP are low triplet energy (2.56 eV),<sup>42</sup> unbalanced injection of holes and electrons, and the presence in CBP films of low energy triplet traps which further reduce the emission from the phosphorescent dopant.<sup>43</sup> By combining Cz with electron-transporting moieties, such as oxadiazole (OXD) derivatives, more balanced injection and transport of charges can be achieved. 2-(Biphenyl-4-yl)-5-(*tert*-butylphenyl)-1,3,4-oxadiazole (PBD) and 1,3-bis[(4-*tert*-butylphenyl)-1,3,4-oxadiazolyl]phenylene (OXD-7) are widely used as electron-transporting materials.<sup>44,45</sup> However, both PBD and OXD-7 have low triplet energies (2.46 and 2.56 eV, respectively).<sup>46</sup>

Received: July 18, 2011

Published: September 27, 2011

Scheme 1. Synthetic Route to 5a–5i<sup>a</sup>

<sup>a</sup> i: NH<sub>4</sub>Cl, NaN<sub>3</sub>, DMF, 105 °C (66–78% yields). ii: 3a–3d, pyridine, reflux (47–85% yields). iii: carbazole (for 5a–g) or 2,7-dimethoxycarbazole (for 5h, i), K<sub>2</sub>CO<sub>3</sub>, DMSO, 150 °C (45–60% yields).

Scheme 2. Synthetic Route to 7a,7b<sup>a</sup>

<sup>a</sup> i: carbazole (for 7a) or 2,7-dimethoxycarbazole (for 7b), K<sub>2</sub>CO<sub>3</sub>, DMSO, 150 °C (61–73% yields).

To achieve the goal of high triplet energy in a bipolar molecule, both the hole- and electron-transporting fragments should possess high triplet energy.

The focus of the current work is the rational design, synthesis, and photophysics of a new series of Cz–OXD dyad molecules 5a–5i and 7a,b in which the topology and electronic properties are systematically varied by chemical modification. Cyclic voltammetric data, DFT calculations, and X-ray crystal structures are also presented. Our Cz–OXD dyads are structurally different from those reported by Thomas et al.<sup>47</sup> and Guan et al.<sup>48</sup> and the Cz–OXD–Cz triad systems studied by Ma et al.<sup>49,50</sup> Furthermore, these authors<sup>47–50</sup> did not report systematic variations to probe structure/property relationships. Our study sheds new light on the interplay of electronic and conformational effects in fluorescent bipolar molecules, and we demonstrate a strategy for precisely tuning the triplet level of the molecule while at the same time limiting the increase in the singlet energy, both of which are vital for the design of useable device materials.

## RESULTS AND DISCUSSION

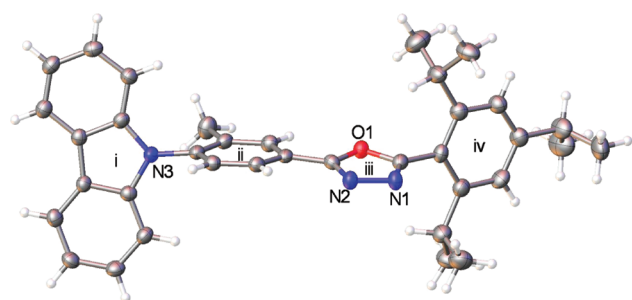
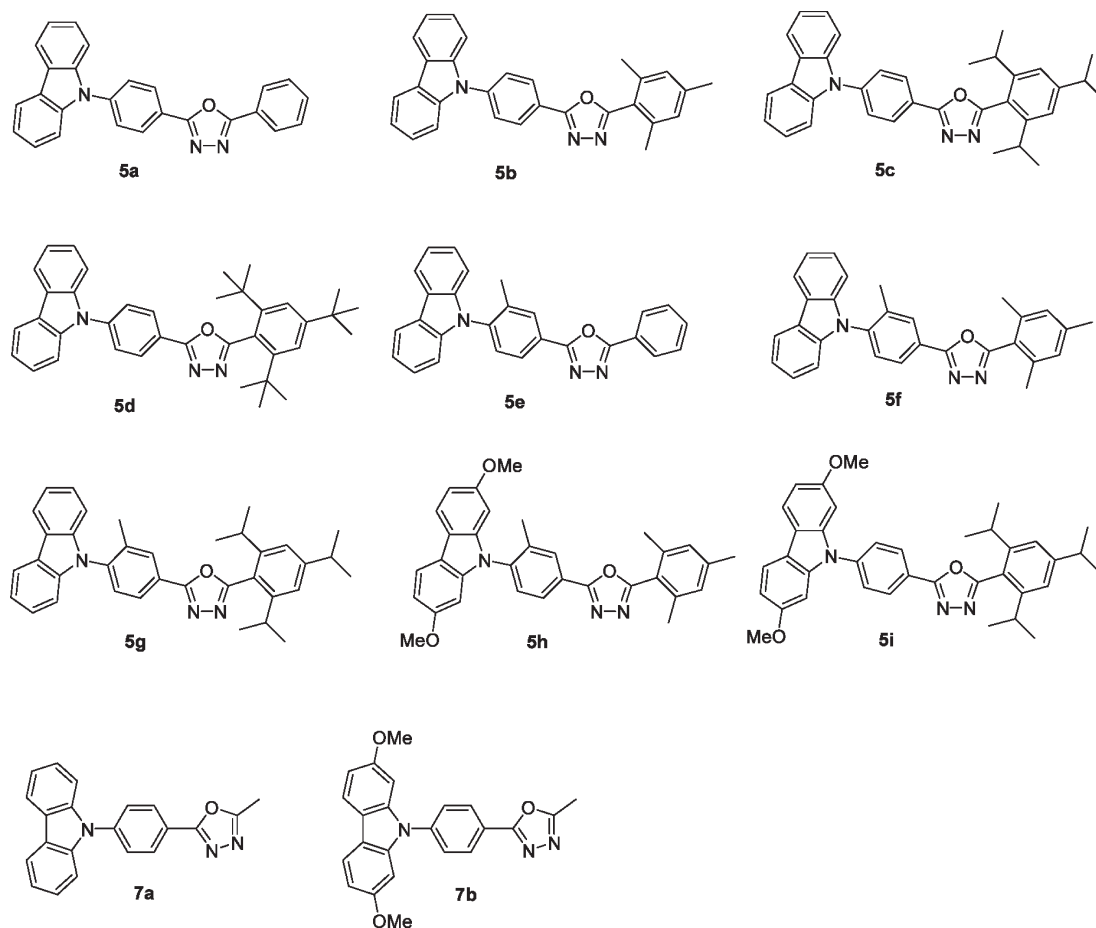
**Molecular Design and Syntheses.** Our targets were 5a–5i and 7a,b in which the torsion angles are systematically varied by alkyl substitution on one, or both, of the phenyl rings of the diphenyl–OXD portion of the molecules. Schemes 1 and 2 outline the routes used for their synthesis, based on tetrazole

precursors.<sup>51</sup> Benzonitrile derivatives 1a and 1b were converted into 2a<sup>52,53</sup> and 2b, which were reacted with 3a–3d in refluxing pyridine to afford 4a–4g. In the final step, S<sub>N</sub>Ar reactions of carbazole or 2,7-dimethoxycarbazole at the C–F bond of 4a–g gave 5a–i. Comparable reactions of 6<sup>54</sup> gave 7a and 7b. All reactions proceeded in moderate to high yields. The structures of the 11 compounds studied in this work are shown in Chart 1.

**X-ray Crystallography.** Single-crystal X-ray diffraction studies were performed on 5c,d,g and 7a to probe the effects of substitution on the inter-ring twist angles (see Figure 1 for 5g and the Supporting Information for the other structures). The twist angle between the essentially planar carbazole group (i) and the benzene ring (ii) is similar in 5c (53.8°), 5d (58.3°), and 7a (54.1°), whereas in 5g it widens to 82.2° due to the methyl substituent at ring ii (Table 1). The twist between the oxadiazole ring (iii) and the benzene ring (iv) is also large due to bulky *peri*-substituents at the latter; it is somewhat larger in the *tert*-butyl-substituted 5d (86.3°) than in *iso*-propyl-substituted 5c (77.4°) and 5g (78.5°). The twist between rings ii and iii varies erratically, viz., 4.3° in 5c, 22.5° in 5d, 11.8° in 5g, and 1.6° in 7a, probably due to packing effects. A search of the May 2011 issue of the CSD<sup>55</sup> revealed 130 organic structures with 242 unique oxadiazolyl–phenyl links without *peri*-substituents at the phenyl ring or other important steric hindrances; the twist angle ranges from 0 to 31° with the average of 8.5(4)°. In these cases, this twist is not big enough to prevent conjugation, unlike the new systems described herein.

**Photophysical Studies.** *A. Photophysics in Fluid Solution.* The data are presented in Table 1. The bipolar compounds investigated in this work show excited state intramolecular charge transfer (ICT), with the carbazole moiety acting as the donor and the oxadiazole as the acceptor. Figure 2a shows the absorption and emission spectra of 5a in nonpolar methylcyclohexane (MCH) and polar ethanol (EtOH). Similar data for the other compounds in Chart 1 are shown in the Supporting Information (Figure S5). While the effect of solvent polarity on the absorption spectrum of 5a is minimal, the fluorescence spectrum in EtOH is significantly broadened and red-shifted when compared with the emission obtained in MCH. The enhanced

Chart 1. Structures of Bipolar Compounds 5a–5i and 7a,b Studied in This Work



**Figure 1.** X-ray molecular structure of 5g, showing thermal ellipsoids of 50% probability. Twist angles ( $^{\circ}$ ): i/ii 82.2; ii/iii 11.8; iii/iv 78.5.

excited state dipole moment of the solute upon excitation induces local dipole–dipole interactions that force the reorientation of the polar solvent molecules around the excited solute. This is accompanied by the molecular structural relaxation and gives rise to inhomogeneous broadening of the fluorescence spectrum with emission occurring from a relaxed state at lower energy. We have previously elucidated this type of behavior in ICT systems.<sup>56</sup>

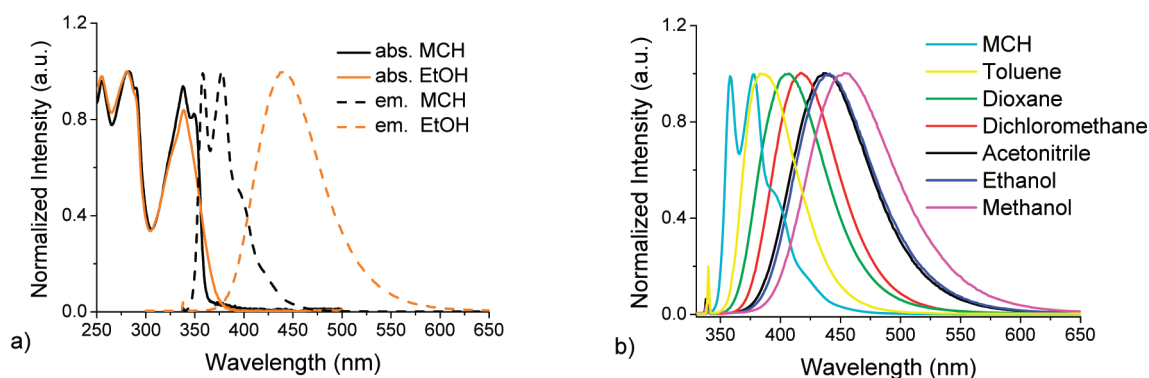
With increasing solvent polarity, the energy of the emissive relaxed state further decreases, giving a sequential red shift of the emission spectra of 5a (Figure 2b). Comparable data for 5i are shown in Figure S6 in the Supporting Information.

The fluorescence lifetime of 5a in nonpolar MCH is well described by a single exponential decay with  $\tau = 1.43$  ns (Figure 3a). However, in ethanol, due to the more complex excited state dynamics, emission decays can only be fitted with a sum of three exponentials, with a fast decay around 20 ps, an intermediate component with 86 ps, and a longer decay term of 4.75 ns (using a global analysis). At 400 nm, the emission rapidly decays, and the importance of the long component is residual; however, at 500 nm, the emission first builds in and is then followed by the long decay (Figure 3b). The pre-exponential amplitude associated with the longer decay component (4.75 ns) is positive, independent of the emission wavelength. This component appears always as a decay term and clearly represents the lifetime of the emissive relaxed state. The two fast decay components around 20 and 86 ps appear with positive pre-exponential amplitudes at shorter wavelengths, so they represent decay components, but at longer emission wavelengths both appear with negative pre-exponential amplitudes, in agreement with the emission build-in observed in Figure 3b. These components appearing as emission decay at shorter wavelengths (positive amplitudes) and as an emission rise time at longer wavelengths (negative amplitudes) are clearly associated with the excited state relaxation described above. Local dipole–dipole interactions occurring during the solute excited state lifetime lead to a red shift of the fluorescence spectrum as a function of time, and this causes the fluorescence intensity collected at a constant wavelength to drop on the high-energy side of the

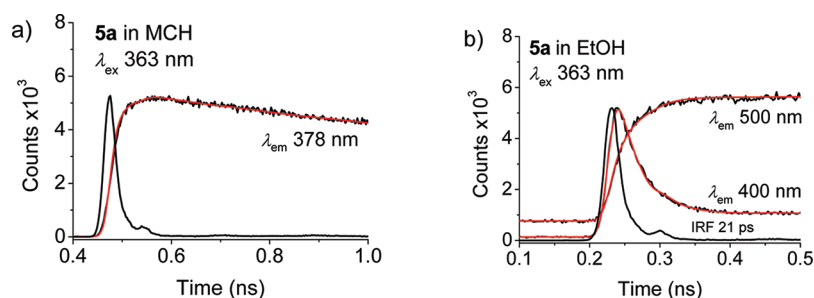
Table 1. Structural, Photophysical, and Solution Electrochemical Data

compound	calculated twist angles between rings		observed twist angle between rings (i) and (ii); (ii) and (iii); (iii) and (iv) ( $^{\circ}$ ) <sup>a</sup>	$\lambda_{\max}$ (nm) absorption, extinction coefficient in PhMe ( $M^{-1} cm^{-1}$ ), 293 K		$\lambda_{\max}$ (nm) emission, in PhMe, 293 K <sup>c</sup>	$\lambda_{\max}$ (nm) emission, in EtOH, 293 K <sup>d</sup>	$\Phi_{PL}$ , <sup>e</sup> in PhMe, 293 K	triplet energy, solid solution		singlet energy, solid solution		$E_S - E_T$ (eV)	LUMO (eV) <sup>g</sup>	HOMO (eV) <sup>h</sup>	$E_{\text{onset/peak}}$ (V) <sup>f</sup>
	(i) and (ii); (ii) and (iii); (iii) and (iv) ( $^{\circ}$ ) <sup>a</sup>	(i) and (ii); (ii) and (iii); (iii) and (iv) ( $^{\circ}$ ) <sup>a</sup>		$\lambda_{\max}$ (nm)	extinction coefficient in PhMe ( $M^{-1} cm^{-1}$ ), 293 K				$E_T$ (eV), 14 K <sup>f</sup>	$E_S$ (eV), 293 K <sup>f</sup>	$E_S$ (eV), 293 K <sup>f</sup>	$E_S$ (eV), 293 K <sup>f</sup>				
<b>5a</b>	51.8/0.2/0			340, 22500		387	440	0.57	2.64	3.42	3.42	0.78	-2.20	-5.62 (-5.60)	0.82/0.96	
<b>5b</b>	52.2/1.4/52.3			340, 21000		379	435	0.59	2.67	3.45	3.45	0.78	-2.20	-5.65 (-5.63)	0.85/1.05	
<b>5c</b>	52.5/0.1/84.2	53.8/4.3/77.4		340, 22300		377	435	0.61	2.73	3.50	3.50	0.77	-2.14	-5.64 (-5.66)	0.84/1.05	
<b>5d</b>	52.8/0.2/88.7	58.3/22.5/86.3		340, 20400		376	432	0.62	2.76	3.52	3.52	0.76	-2.07	-5.59 (-5.61)	0.79/1.03	
<b>5e</b>	83.0/1.1/0			339, 14500		382	445	0.56	2.66	3.47	3.47	0.81	-2.04	-5.66 (-5.68)	0.86/0.93	
<b>5f</b>	70.7/0.3/53.8			339, 13500		377	440	0.44	2.73	3.45	3.45	0.72	-2.23	-5.68 (-5.73)	0.88/1.09	
<b>5g</b>	73.1/0.5/82.6	82.2/11.8/78.5		339, 11800		375	440	0.38	2.78	3.56	3.56	0.78	-2.11	-5.67 (-5.65)	0.87/1.05	
<b>5h</b>	69.2/2.9/50.3			319, 22800		436	-	0.06	2.73	3.37	3.37	0.64	-2.16	-5.53 (-5.55)	0.73/0.95	
<b>5i</b>	52.2/0.4/84.8			319, 21900		437	-	0.03	2.73	3.37	3.37	0.63	-2.24	-5.61 (-5.58)	0.66/0.81	
<b>7a</b>	52.1/1.0	54.1/1.6		340, 18200		372	440	0.55	2.76	3.52	3.52	0.76	-2.10	-5.62 (-5.67)	0.82/0.98	
<b>7b</b>	51.5/1.1			319, 21400		428	-	0.06	2.76	3.37	3.37	0.61	-2.06	-5.43 (-5.47)	0.63/0.83	

<sup>a</sup> Data from geometry optimizations at the B3LYP/6-31G(d) level of theory. <sup>b</sup> From X-ray crystal structural data. <sup>c</sup>  $\lambda_{\text{ex}} = 363$  nm. <sup>d</sup>  $\lambda_{\text{ex}} = 363$  nm. Emission of **5h**, **5i**, and **7b** in EtOH is so weak that  $\lambda_{\text{em}}$  values could not be reliably obtained. <sup>e</sup> Photoluminescence quantum yield; error  $\pm 15\%$  (for **5h**, **5i**, **7b** error  $\pm 50\%$ );  $\lambda_{\text{ex}} 340$  nm. <sup>f</sup> Error  $\pm 0.01$  eV. <sup>g</sup> Obtained from the HOMO (CV data) + optical band gap (onset of absorption in PhMe). <sup>h</sup> Obtained from the CV data. The first value for each compound in this column is calculated from the onset of the oxidative wave; the values in brackets are calculated from the half-wave potential on the oxidative scan. <sup>i</sup> Obtained by cyclic voltammetry. Data reported are for the first scan.



**Figure 2.** (a) Normalized absorption and emission spectra of **5a** in MCH and EtOH solution at 293 K. (b) Emission spectra of **5a** at 293 K in solvents with different polarity.



**Figure 3.** (a) Fluorescence decay of **5a** in MCH at 293 K with emission collected at 378 nm. (b) Fluorescence decay of **5a** in ethanol at 293 K with emission collected at 400 and 500 nm. Excitation wavelength at 363 nm in both cases.

**Table 2. Lifetime Data for Compounds**

compound	phosphorescence <sup>a</sup>		fluorescence <sup>b</sup>			$\chi^2$
	$\tau_1$ (ms)	$\tau_1$ (ns) ( $A_1$ )	$\tau_2$ (ns) ( $A_2$ )	$\tau_3$ (ns) ( $A_3$ )		
<b>5a</b>	416	4.71 (0.42)	0.083 (0.24)	0.023 (0.34)	1.20	
<b>5b</b>	454	4.92 (0.42)	0.112 (0.17)	0.029 (0.41)	1.08	
<b>5c</b>	740	5.01 (0.43)	0.139 (0.16)	0.028 (0.41)	1.11	
<b>5d</b>	858	4.93 (0.45)	0.127 (0.19)	0.028 (0.36)	1.10	
<b>5e</b>	448	4.72 (0.38)	0.087 (0.19)	0.018 (0.43)	1.19	
<b>5f</b>	546	4.65 (0.41)	0.112 (0.21)	0.025 (0.38)	1.01	
<b>5g</b>	627	4.51 (0.32)	0.171 (0.16)	0.029 (0.52)	1.03	
<b>5h</b>	641	-	-	-	-	
<b>5i</b>	709	-	-	-	-	
<b>7a</b>	686	5.01 (0.41)	0.065 (0.25)	0.008 (0.34)	1.10	
<b>7b</b>	626	-	-	-	-	

<sup>a</sup> Measured in zeonex at 14 K,  $\lambda_{\text{ex}} = 355$  nm. <sup>b</sup> Measured in ethanol at 293 K,  $\lambda_{\text{ex}} = 363$  nm, single wavelength analysis of decays collected at  $\lambda_{\text{em}}$  440 nm. Fluorescence of **5h**, **5i**, and **7b** in EtOH is so weak that lifetimes could not be reliably obtained.

emission spectrum and to build in at longer wavelengths.<sup>57</sup> The fluorescence lifetime data for all compounds are shown in Table 2.

Interestingly, while compounds **5a–5g** and **7a** show strong emission in polar and nonpolar solvents (e.g.,  $\Phi_{\text{PL}} 0.38–0.62$  in PhMe), the dimethoxy-substituted compounds **5h**, **5i**, and **7b** show almost no emission in ethanol and low  $\Phi_{\text{PL}}$  values (0.03–0.06) in toluene (Table 1) suggesting an enhanced triplet

yield in these derivatives. This has been confirmed by temperature dependence studies of the emission for **5a** and **5i**.

The temperature dependence of emission of **5a** shows a shift to shorter wavelengths with decreasing temperature, as a result of a slower solvent reorganization around the excited solute at low temperatures, but no further emissive state is observed (Figure 4a). This is a common observation in compounds showing excited state ICT: decreasing the temperature makes the solvent more viscous, and the solvent reorganization takes a longer time to occur; as a consequence, the emission from nonrelaxed states starts to compete, and progressively, as the temperature drops, emission occurs from a state closer in energy to the Franck–Condon state.<sup>57</sup>

In contrast to strong fluorescence, emission from the triplet state is usually not observed in steady state conditions. Phosphorescence is normally much weaker than fluorescence, which makes phosphorescence difficult to observe. Acquisition-gated methods have generally been needed to collect phosphorescence spectra; these use a delay time between the excitation pulse and the emission acquisition to separate the weak phosphorescence and the strong fluorescence signals.<sup>58</sup> However, in the case of compound **5i**, phosphorescence emission is clearly observed coexisting with fluorescence in a simple steady-state emission acquisition at low temperatures (Figure 4b). The decreased emission yield observed at room temperature and the strong phosphorescence observed at low temperature strongly suggest an increase in the triplet yield of the dimethoxy-substituted compounds **5h**, **5i**, and **7b**.

**B. Photophysics in Solid Solution.** In Figure 5, the normalized phosphorescence and fluorescence spectra of **5a**, **5b**, **5c**, and **5d** in a zeonex matrix are depicted. The triplet levels of all four compounds are higher than those of CBP, PBD, and OXD-7 (see above), and the level increases sequentially (**5a** < **5b** < **5c** < **5d**)

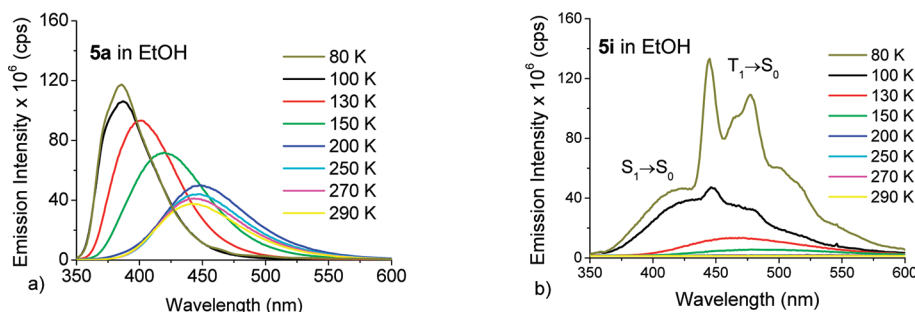


Figure 4. Emission spectra of (a) **5a** and (b) **5i** in EtOH solution as a function of temperature.

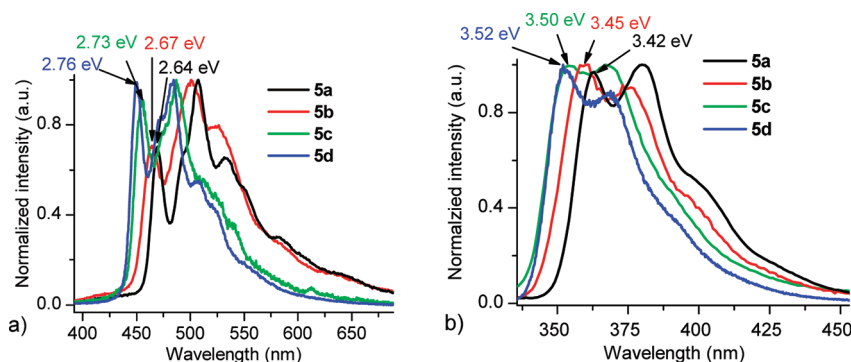


Figure 5. (a) Normalized phosphorescence at 14 K and (b) normalized fluorescence spectra at 293 K of **5a**, **5b**, **5c**, and **5d** in zeonex. Peak energies (triplet and singlet levels, respectively) are indicated on the spectra.

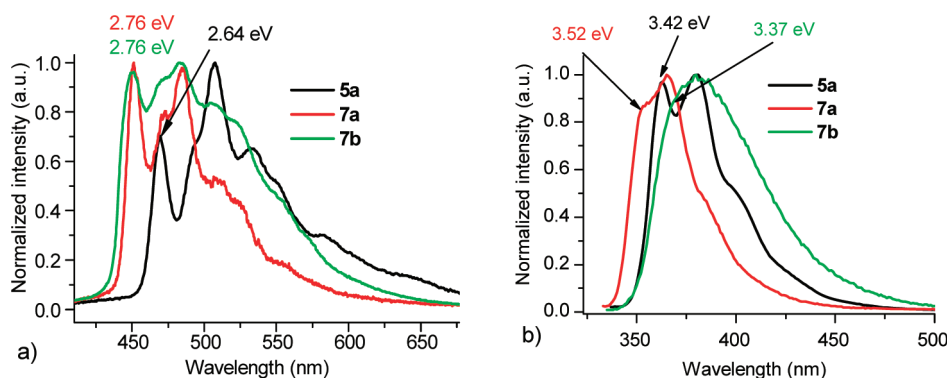


Figure 6. (a) Normalized phosphorescence at 14 K and (b) normalized fluorescence spectra at 293 K of **5a**, **7a**, and **7b** in zeonex. Peak energies (triplet and singlet levels, respectively) are indicated on the spectra.

with increasing torsion angle between rings iii and iv (Table 1) due to a reduction of  $\pi$ -conjugation in this part of the molecules. The singlet levels are similarly raised (**5a** < **5b** < **5c** < **5d**), and the lower-energy absorption edge blue shifts in toluene solution in the sequence **5a** < **5b** < **5c**  $\approx$  **5d** with increasing torsion angles (Figure S9 in the Supporting Information).

Figure 6 shows a comparison of **5a**, **7a**, and **7b**. Replacing the terminal phenyl ring iv with a methyl substituent has the same effect in raising the triplet and singlet energy levels as introducing a large torsion angle between rings iii and iv, for example, with *t*-butyl groups (for both **5d** and **7a**:  $E_T = 2.76$  eV;  $E_S = 3.52$  eV). This further confirms that effective reduction of  $\pi$ -conjugation in the diphenyl–OXD moieties is responsible for increasing both the triplet and singlet levels by ca. 0.1 eV, compared with the parent compound **5a**.

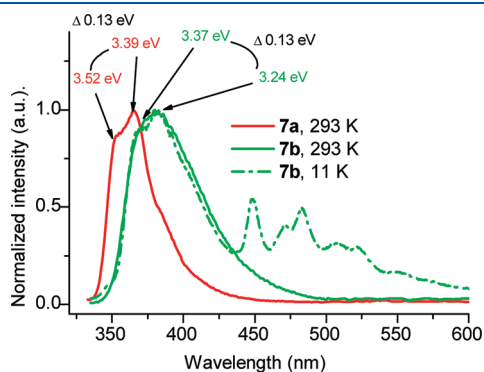
The introduction of electron-donating 2,7-dimethoxy substituents onto the Cz moiety (**7b**) shifts  $E_S$  by 0.15 eV to the red in comparison with **7a**, although  $E_T$  is unaffected, which means that the singlet–triplet gap in **7b** is reduced to 0.61 eV.

The room-temperature steady state fluorescence spectrum of **7b** is very broad (Figure 6b). This could be due to the introduction of new vibrational modes arising from the methoxy substituents and/or an enhanced ICT contribution because dimethoxycarbazole is a stronger electron donor than carbazole. For the spectrum recorded at 11 K (Figure 7), the features are more resolved, and the difference between the vibrational shoulders of **7a** at 293 K and **7b** at 11 K is the same (0.13 eV) with a red shift observed for **7b**. Thus, 3.37 eV, which is the highest-energy shoulder in the fluorescence peak at 11 K, was taken as the singlet level for **7b**. In the 11 K spectrum, in the range 440–600 nm,

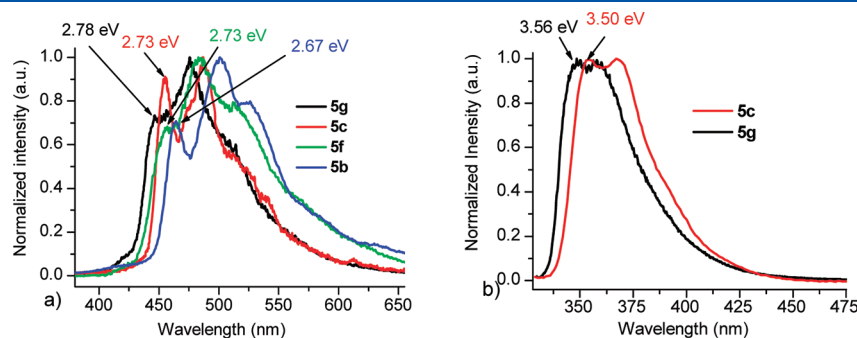
phosphorescence in a steady state *not* gated spectrum can be observed, indicating especially efficient phosphorescence emission. Similarly broadened spectra at room temperature are observed for the dimethoxycarbazole derivatives **5h** and **5i** compared to **5f** and **5c**, respectively (Figure S7 in Supporting Information) with a red shift in  $E_S$  and no change in  $E_T$ . By analogy with compound **7b**, singlet levels of **5h** and **5i** were determined to be 3.37 eV.

From the above data, we conclude that the triplet excited state is located mostly on the diphenyloxadiazole unit of the molecules as the methoxy substituents on the Cz unit do not affect the triplet level. This is reasonable as carbazole has  $E_T = 3.05$  eV,<sup>38</sup> whereas diaryl–OXD derivatives have lower values; e.g., PBD has  $E_T = 2.46$  eV,<sup>46</sup> and OXD-7 has  $E_T = 2.56$  eV.<sup>46</sup> The excited triplet state will be located primarily on the fragment with the lower triplet energy level. This means that changes in  $E_T$  can be engineered by chemical modification to the diaryl–OXD moiety (twisting it, reducing conjugation, etc.), whereas modification to the Cz moiety will change  $E_S$  but not  $E_T$ .

Furthermore, we observe an increase of both triplet and singlet levels when a methyl group is introduced on the phenyl ring (ring ii) adjacent to the Cz unit (structures **5e–h**) (Figure 8). For **5e**,  $E_T$  shifts by only 0.02 eV (Figure S8 in SI) to the blue compared to **5a**, whereas the singlet state shifts considerably more, by 0.05 eV (Figure 8b). Compound **5g** has a larger blue shift of  $E_T$  in comparison with **5c** (0.05 eV for  $E_T$  and 0.06 eV shift for  $E_S$ ). The phosphorescence of **5f** blue shifts by ca. 0.06 eV in comparison with **5b**. The  $E_S$  of **5f** and **5b** are the same (3.45 eV) if the highest-energy shoulder in the fluorescence spectra is taken as the singlet level. However, the vibronics for **5f** are not as well resolved as the vibronic shoulders of **5b**, thus the onset difference



**Figure 7.** Normalized phosphorescence spectra of **7a** at 293 K and **7b** at 293 and 11 K in zeonex.



**Figure 8.** (a) Normalized phosphorescence spectra of **5b**, **5c**, **5f**, and **5g** at 14 K and (b) normalized fluorescence spectra of **5c** and **5g** at 293 K in zeonex. Peak energies (triplet and singlet levels, respectively) are indicated on the spectra.

would be a better indicator of the singlet level difference for these compounds which is  $\sim 0.03$  eV (Figure S8 in Supporting Information).

For the compounds where a methyl group is introduced on ring ii, in both the phosphorescence and the fluorescence spectra the vibronic shoulders are less resolved, compared to analogues without a methyl group: compare the spectra in Figure 5 (no Me group on ring ii) with the spectra of **5f** and **5g** (with a Me group) in Figure 8a. Figure 8b shows that the fluorescence of **5g** is similarly blue-shifted by methyl substitution on ring ii compared to the unsubstituted analogue **5c**.

The triplet state lifetime ( $\tau_1$ ) (Table 2) for all of the compounds exceeds 400 ms and decays exponentially at 15 K, which is reasonable bearing in mind that molecules in a zeonex matrix are isolated ( $1 \times 10^{-4}$  mass to mass ratio) thus reducing the probability of any type of energy transfer.<sup>59</sup> The triplet lifetime increases with an increase of the torsion angle (rings iii/iv) and with an increase in  $E_T$ , i.e.,  $\tau_1$  **5a** < **5b** < **5c** < **5d**. A similar progression is observed in the series with a methyl substituent on ring ii:  $\tau_1$  **5e** < **5f** < **5g**. This is consistent with Kasha's rule for radiationless transitions which states that with an increase of the bandgap there is a decrease in the decay rate of radiationless transitions (i.e., the overall lifetime increases).<sup>60</sup>

Cyclic voltammetric data for **5a–i** and **7a,b** in dichloromethane solution are shown in Table 1. Compounds show irreversible oxidation waves on the first scan leading to the radical cation at ca. 0.8 V, which is typical of carbazoles.<sup>61</sup> On subsequent scans, for most of the compounds, an additional peak appears at ca. 0.5–0.6 V, most likely resulting from electrochemical dimerization at C3 and C6 of the carbazole unit.<sup>62</sup> The 2,7-dimethoxy substituents on **5h**, **5i**, and **7b** lower the oxidation potential by 100–200 mV due to stabilization of the radical cation species. Cyclic voltammograms are shown in the Supporting Information. No reduction waves could be resolved on scanning to  $-2.0$  V. Both the onset potential<sup>49</sup> and the half-wave potential<sup>24</sup> of the oxidative wave (the latter approximating to a 1:1 mixture of neutral and oxidized species) are routinely used to estimate HOMO energy levels.<sup>63</sup> The calculations using both methods give values consistent to within  $\pm 0.05$  eV for each compound (Table 1).

DFT calculations (see the Supporting Information) show that for each compound the HOMO is located predominantly on the carbazole moiety, whereas the LUMO is predominantly on the phenyl/diphenyloxadiazole moiety. The LUMO density on the terminal phenyl ring (ring iv in Figure 1) decreases in the sequence **5a** > **5b** > **5c** > **5d**, as the increasing steric bulk of the substituents on that ring leads to an increased dihedral angle

between rings iii and iv and a reduction of the  $\pi$ -conjugation with the oxadiazole ring iii.

## CONCLUSIONS

A series of Cz–OXD hybrid molecules has been synthesized to evaluate electronic and conformational effects on the singlet and triplet energies. Excited state ICT is observed from the donor carbazole/2,7-dimethoxycarbazole to the acceptor phenyl/diphenyloxadiazole moieties. Introducing more bulky alkyl substituents onto the diphenyloxadiazole fragment systematically increases the singlet and triplet levels and blue shifts the absorption and emission bands. Replacement of the terminal phenyl unit by a methyl group has a similar effect. By introducing methoxy groups at the 2,7-positions of the carbazole moiety, the singlet level is decreased without changing the triplet excited state, thereby reducing the singlet–triplet energy gap. These modifications enable fine-tuning of the photophysical properties in Cz–OXD systems. Notably, we have demonstrated a strategy for precisely tuning the triplet level of a bipolar molecule while at the same time limiting the increase in the singlet energy. These compounds have potential as bipolar hosts in OLEDs. The design features we have developed should aid the search for new charge transfer molecules for fundamental studies and for a range of optoelectronic applications.

## EXPERIMENTAL SECTION

**General Experimental Methods.** All air-sensitive reactions were conducted under a blanket of argon which was dried by passage through a column of phosphorus pentoxide. All commercial chemicals were used without further purification. Solvents were dried and degassed following standard procedures. Column chromatography was carried out using 40–60  $\mu$ m mesh silica.

For phosphorescence and fluorescence measurements, the sample was doped into zeonex, which is a commercial host polymer matrix. The concentration in zeonex was  $\sim 1 \times 10^{-4}$  mass to mass ratio. The zeonex solution of the materials was drop cast onto sapphire substrates of 12 mm diameter. Gated luminescence and lifetime measurements were made using a system consisting of an excitation source and a pulsed YAG laser emitting at 355 nm. Samples were excited at a 45° angle to the substrate plane, and the energy of each pulse was  $\sim 25 \mu$ J. Emission was focused onto a spectrograph and detected on a sensitive gated ICCD camera with subnanosecond resolution. Decay measurements were performed by logarithmically increasing gate and delay times; more details can be found elsewhere.<sup>64</sup> For low-temperature measurements (down to 11 K), samples were placed in the displax cryostat. Absorption spectra were recorded by using an absorption spectrophotometer in dilute toluene solutions (in the range of  $1 \times 10^{-5}$  molar concentration). Steady state luminescence emission was recorded using a commercial spectrofluorimeter. Singlet and triplet levels were determined by taking the highest-energy vibronic shoulder in fluorescence and phosphorescence spectra, respectively. The accuracy of singlet and triplet level determination was evaluated to be  $\pm 0.01$  eV. Solution photoluminescence quantum yields were determined in toluene and recorded in comparison with quinine sulfate in  $\text{H}_2\text{SO}_4$  (1 M) and with 9,10-diphenylanthracene in cyclohexane as standards; the error for the PLQY is  $\pm 15\%$ , except for compounds with PLQY values  $< 0.1$  where the error is  $\pm 50\%$ .

Cyclic voltammograms were recorded in dichloromethane at a scan rate of 100 mV  $\text{s}^{-1}$  for five cycles at room temperature using an airtight single-compartment three-electrode cell equipped with a Pt disk working electrode, Pt wire counter electrode, and Pt wire pseudoreference electrode. The cell was connected to a computer-controlled potentiostat.

The solutions contained the compound together with *n*-Bu<sub>4</sub>NPF<sub>6</sub> (0.1 M) as the supporting electrolyte. All potentials are reported with reference to an internal standard of the ferrocene/ferrocenium couple ( $\text{Fc}/\text{Fc}^+ = 0.00$  V).

**Synthesis.** Compounds **4a**<sup>65</sup> and **4b–d**<sup>66</sup> were synthesized as described previously.

**5-(4-Fluoro-3-methylphenyl)-1H-tetrazole (2b).** A solution of 4-fluoro-3-methylbenzonitrile **1b** (1.50 g, 11.1 mmol), sodium azide (0.80 g, 12.2 mmol), ammonium chloride (0.65 g, 12.2 mmol), and anhydrous DMF (30 mL) was refluxed overnight. The solution was cooled and water added, and then the solution was acidified with dilute HCl to precipitate **2b** as a pale yellow solid (1.32 g, 66%). Mp: 200.5–201.8 °C. Anal. Calcd for C<sub>8</sub>H<sub>7</sub>FN<sub>4</sub>: C, 53.93; H, 3.96; N, 31.45. Found: C, 53.81; H, 4.00; N, 31.49.  $\delta_{\text{H}}$  (700 MHz, DMSO-*d*<sub>6</sub>) 7.96 (1H, d, *J* 7.1), 7.86 (1H, d, *J* 5.3), 7.37 (1H, t, *J* 9.1), 2.31 (3H, s) (NH not observed).  $\delta_{\text{C}}$  (176 MHz, DMSO-*d*<sub>6</sub>) 162.6 (d, *J* 248.3), 130.9 (d, *J* 5.8), 127.2 (d, *J* 9.0), 126.2 (d, *J* 18.1), 116.6 (d, *J* 23.2), 110.0, 14.6 (d, *J* 3.2). MS (EI): *m/z* (EI) 177.9 (*M*<sup>+</sup>, 20%), 149.7 (100%).

**2-(4-Fluoro-3-methylphenyl)-5-phenyl-1,3,4-oxadiazole (4e).** A solution of **2b** (0.33 g, 1.7 mmol), **3a** (0.28 g, 2.0 mmol), and pyridine (5 mL) was refluxed overnight. The solution was cooled, and water was added. The precipitate was collected, dried, and purified by column chromatography (SiO<sub>2</sub>, eluent DCM/EtOAc 19:1 v/v) followed by recrystallization from ethanol to give **4e** (0.36 g, 84%) as a white solid. Mp: 139.5–140.8 °C. Anal. Calcd for C<sub>15</sub>H<sub>11</sub>FN<sub>2</sub>O: C, 70.86; H, 4.36; N, 11.02. Found: C, 70.93; H, 4.24; N, 11.05.  $\delta_{\text{H}}$  (700 MHz, CDCl<sub>3</sub>) 8.14 (2H, dd, *J* 10.0, 16.6), 8.00 (1H, d, *J* 7.3), 7.98–7.90 (1H, m), 7.63–7.44 (3H, m), 7.15 (1H, t, *J* 8.9), 2.37 (3H, s).  $\delta_{\text{C}}$  (176 MHz, CDCl<sub>3</sub>) 164.5, 164.0, 163.4 (d, *J* 251.9), 131.7, 130.4 (d, *J* 6.0), 129.1, 126.9, 126.5 (d, *J* 8.9), 126.2 (d, *J* 18.2), 123.9, 119.9 (d, *J* 3.5), 116.0 (d, *J* 23.4), 14.5 (d, *J* 3.5). MS (EI): *m/z* 254.0 (*M*<sup>+</sup>, 100%).

**2-(4-Fluoro-3-methylphenyl)-5-(2,4,6-trimethylphenyl)-1,3,4-oxadiazole (4f).** Following the procedure for **4e**, **2b** (0.30 g, 1.7 mmol), **3b** (0.360 g, 2.0 mmol), and pyridine (5 mL) gave **4f** (0.28 g, 56%) as a white solid. Mp: 93.7–94.8 °C. Anal. Calcd for C<sub>18</sub>H<sub>17</sub>FN<sub>2</sub>O: C, 72.95; H, 5.78; N, 9.45. Found: C, 72.64; H, 5.90; N, 9.50.  $\delta_{\text{H}}$  (700 MHz, CDCl<sub>3</sub>) 7.96 (1H, d, *J* 7.1), 7.89 (1H, dd, *J* 3.9, 7.0), 7.14 (1H, t, *J* 8.9), 6.98 (2H, s), 2.35 (3H, s), 2.34 (3H, s), 2.30 (6H, s).  $\delta_{\text{C}}$  (176 MHz, CDCl<sub>3</sub>) 164.2, 164.2, 164.1, 163.8, 162.6, 141.0, 138.7, 130.3, 130.3, 128.8, 126.4, 126.3, 126.1, 121.0, 120.0, 116.0, 115.9, 30.9, 21.2, 20.5. MS (EI): *m/z* 296.0 (*M*<sup>+</sup>, 70%), 146.7 (100%).

**2-(4-Fluoro-3-methylphenyl)-5-(2,4,6-trisopropylphenyl)-1,3,4-oxadiazole (4g).** Following the procedure for **4e**, **2b** (0.20 g, 1.1 mmol), **3c** (0.30 g, 1.1 mmol) and pyridine (5 mL) gave **4g** (0.29 g, 70%) as a white solid. Mp: 99.3–101.0 °C. Anal. Calcd for C<sub>24</sub>H<sub>29</sub>FN<sub>2</sub>O: C, 75.76; H, 7.68; N, 7.36. Found: C, 75.42; H, 7.60; N, 7.60.  $\delta_{\text{H}}$  (700 MHz, CDCl<sub>3</sub>) 7.94 (1H, d, *J* 7.0), 7.88 (1H, dd, *J* 4.1, 7.1), 7.16–7.09 (3H, m), 2.96 (1H, dt, *J* 6.9), 2.64 (2H, hept, *J* 6.8), 2.35 (3H, s), 1.29 (6H, d, *J* 6.9), 1.20 (12H, d, *J* 6.8).  $\delta_{\text{C}}$  (176 MHz, CDCl<sub>3</sub>) 164.4, 163.8, 163.4 (d, *J* 251.7), 152.4, 149.4, 130.3 (d, *J* 6.0), 126.4 (d, *J* 8.9), 126.2 (d, *J* 18.2), 121.2, 120.1 (d, *J* 3.9), 119.65, 116.0 (d, *J* 23.4), 34.6, 31.5, 24.1, 23.9, 14.5 (d, *J* 3.4). MS (EI): *m/z* 380.1 (*M*<sup>+</sup>, 15%), 230.5 (100%).

**2-[4-(9H-Carbazol-9-yl)phenyl]-5-phenyl-1,3,4-oxadiazole (5a).** A solution of **4a** (0.22 g, 0.6 mmol), carbazole (0.10 g, 0.6 mmol), K<sub>2</sub>CO<sub>3</sub> (200 mg), and DMSO (10 mL) was heated at 150 °C overnight. The solution was cooled, and water was added. The mixture was extracted with DCM, and the organic layer was separated and dried over MgSO<sub>4</sub>. A brown solid which was obtained after removing the solvent was purified by column chromatography (SiO<sub>2</sub>, eluent DCM/EtOAc 98:2 v/v) followed by recrystallization from EtOH yielding compound **5a** (0.13 g, 55%) as a white solid. Mp: 223.5–224.8 °C. Anal. Calcd for C<sub>26</sub>H<sub>17</sub>N<sub>3</sub>O: C, 80.60; H, 4.42; N, 10.85. Found: C, 80.61; H, 4.40; N, 10.83.  $\delta_{\text{H}}$  (500 MHz, CDCl<sub>3</sub>) 8.46–8.39 (2H, m), 8.25–8.19 (2H, m), 8.18 (2H, d, *J* 7.7), 7.85–7.78 (2H, m), 7.64–7.51 (5H, m), 7.50–7.44 (2H, m), 7.38–7.32 (2H, m).  $\delta_{\text{C}}$  (126 MHz, CDCl<sub>3</sub>) 165.1, 159.8, 141.2, 140.5, 132.2, 129.5, 128.8,



Table 3. Crystal Data and Experimental Details

compound	5c	5d	5g	7a
CCDC dep. no.	834130	834131	834132	834133
formula	C <sub>35</sub> H <sub>35</sub> N <sub>3</sub> O	C <sub>38</sub> H <sub>41</sub> N <sub>3</sub> O	C <sub>36</sub> H <sub>37</sub> N <sub>3</sub> O	C <sub>21</sub> H <sub>15</sub> N <sub>3</sub> O
Fw	513.66	555.74	527.69	325.36
T (K)	120	120	120	120
crystal system	orthorhombic	orthorhombic	monoclinic	monoclinic
space group (no.)	P2 <sub>1</sub> 2 <sub>1</sub> 2 <sub>1</sub> (#19)	Pna2 <sub>1</sub> (#33)	P2 <sub>1</sub> /c (#14)	P2 <sub>1</sub> /c (#14)
a (Å)	10.5653(9)	11.8018(17)	18.1747(11)	8.1023(12)
b (Å)	15.6361(13)	8.7725(13)	9.1474(6)	28.568(5)
c (Å)	17.4361(15)	30.605(5)	17.9815(13)	7.1293(11)
β (deg)	90	90	96.331(14)	99.235(11)
V (Å <sup>3</sup> )	2880.4(4)	3168.5(8)	2971.2(3)	1628.8(4)
Z	4	4	4	4
D <sub>c</sub> (g cm <sup>-3</sup> )	1.184	1.165	1.180	1.327
μ (mm <sup>-1</sup> )	0.07	0.07	0.07	0.08
no. of reflections total	35449	23732	20234	19154
no. of unique reflections	4636	2838	5223	4330
R <sub>int</sub>	0.031	0.088	0.089	0.043
R <sub>1</sub> <sup>a</sup> [I > 2σ(I)]	0.039	0.053	0.042	0.044
wR <sub>2</sub> <sup>b</sup> (all data)	0.099	0.119	0.097	0.110

$${}^a R_1 = \sum ||F_o| - |F_c|| / \sum |F_o|. \quad {}^b wR_2 = [\sum w(F_o^2 - F_c^2)^2 / \sum w(F_o^2)]^{1/2}.$$

127.5, 127.3, 126.5, 124.1, 122.7, 120.8, 120.7, 109.99, 109.95. MS (EI): *m/z* 387.1 (M<sup>+</sup>, 100%).

2-[4-(9H-Carbazol-9-yl)phenyl]-5-(2,4,6-trimethylphenyl)-1,3,4-oxadiazole (**5b**). Following the procedure for **5a**, **4b** (0.18 g, 0.67 mmol), carbazole (0.11 g, 0.69 mmol), K<sub>2</sub>CO<sub>3</sub> (200 mg), and DMSO (10 mL) gave **5b** (0.16 g, 55%) as a white solid. Mp: 191.8–192.6 °C. Anal. Calcd for C<sub>29</sub>H<sub>23</sub>N<sub>3</sub>O: C, 81.09; H, 5.40; N, 9.78. Found: C, 81.10; H, 5.36; N, 9.76. δ<sub>H</sub> (700 MHz, CDCl<sub>3</sub>) 8.35 (2H, d, J 8.2), 8.15 (2H, d, J 7.5), 7.77 (2H, d, J 8.3), 7.49 (2H, d, J 8.1), 7.43 (2H, t, J 7.6), 7.32 (2H, t, J 7.4), 7.02 (2H, s), 2.36 (9H, s). δ<sub>C</sub> (176 MHz, CDCl<sub>3</sub>) 164.3, 164.1, 141.2, 140.9, 140.3, 138.8, 128.9, 128.5, 127.3, 126.2, 123.8, 122.6, 121.0, 120.6, 120.5, 109.7, 21.3, 20.5. MS (EI): *m/z* 429.1 (M<sup>+</sup>, 100%).

2-[4-(9H-Carbazol-9-yl)phenyl]-5-(2,4,6-triisopropylphenyl)-1,3,4-oxadiazole (**5c**). Following the procedure for **5a**, **4c** (0.50 g, 1.4 mmol), carbazole (0.23 g, 1.4 mmol), K<sub>2</sub>CO<sub>3</sub> (400 mg), and DMSO (20 mL) gave **5c** (0.36 g, 52%) as colorless crystals. Mp: 216.2–217.0 °C. Anal. Calcd for C<sub>35</sub>H<sub>35</sub>N<sub>3</sub>O: C, 81.84; H, 6.87; N, 8.18. Found: C, 81.75; H, 6.88; N, 8.11. δ<sub>H</sub> (700 MHz, CDCl<sub>3</sub>) 8.33 (2H, d, J 8.5), 8.15 (2H, d, J 7.7), 7.77 (2H, d, J 8.5), 7.49 (2H, d, J 8.2), 7.43 (2H, t, J 7.6), 7.32 (2H, t, J 7.4), 7.16 (2H, s), 2.98 (1H, hept, J 7.0), 2.71 (2H, hept, J 6.8), 1.31 (6H, d, J 6.9), 1.25 (12H, d, J 6.8). δ<sub>C</sub> (176 MHz, CDCl<sub>3</sub>) 164.5, 164.1, 152.5, 149.5, 140.9, 140.3, 128.5, 127.3, 126.2, 123.8, 122.7, 121.3, 120.6, 120.5, 119.6, 109.7, 34.6, 31.5, 24.1, 23.9. MS (MALDI+): *m/z* 513.4 (M<sup>+</sup>, 100%). Crystals for X-ray analysis were grown by slowly cooling a solution of **5c** in acetonitrile.

2-[4-(9H-Carbazol-9-yl)phenyl]-5-(2,4,6-tert-butylphenyl)-1,3,4-oxadiazole (**5d**). Following the procedure for **5a**, **4d** (0.10 g, 0.25 mmol), carbazole (0.05 g, 0.30 mmol), K<sub>2</sub>CO<sub>3</sub> (200 mg), and DMSO (20 mL) gave a product which was purified by column chromatography (SiO<sub>2</sub>, eluent DCM/EtOAc 97:3 v/v) followed by recrystallization from acetonitrile to afford **5d** (0.08 g, 59%) as colorless crystals. Mp: 222.0–223.0 °C. Anal. Calcd for C<sub>38</sub>H<sub>41</sub>N<sub>3</sub>O: C, 82.12; H, 7.44; N, 7.56. Found: C, 81.96; H, 7.45; N, 7.54. δ<sub>H</sub> (700 MHz, CDCl<sub>3</sub>) 8.33 (2H, d, J 8.7), 8.15 (2H, d, J 7.1), 7.77 (2H, d, J 8.7), 7.58 (2H, s), 7.51 (2H, d, J 8.2), 7.43 (2H, t, J 7.7), 7.32 (2H, t, J 7.9), 1.39 (9H, s), 1.25 (18H, s). δ<sub>C</sub> (176 MHz, CDCl<sub>3</sub>) 164.9, 163.4, 153.0, 151.6, 140.9, 140.3, 128.4, 127.3, 126.2, 123.8, 122.6, 122.3, 120.6, 120.4, 118.0, 109.7, 37.2, 35.3, 32.3, 31.3. MS (MALDI+): *m/z* 555.3 (M<sup>+</sup>, 100%). Crystals for X-ray analysis were grown by slowly cooling a solution of **5d** in MeCN.

2-[4-(9H-Carbazol-9-yl)-3-methylphenyl]-5-phenyl-1,3,4-oxadiazole (**5e**). Following the procedure for **5a**, **4e** (0.23 g, 0.9 mmol), carbazole (0.15 g, 0.9 mmol), K<sub>2</sub>CO<sub>3</sub> (200 mg), and DMSO (10 mL) gave **5e** (0.19 g, 53%) as a white solid. Mp: 197.1–197.8 °C. Anal. Calcd for C<sub>27</sub>H<sub>19</sub>N<sub>3</sub>O: C, 80.78; H, 4.77; N, 10.47. Found: C, 80.36; H, 4.71; N, 10.31. δ<sub>H</sub> (700 MHz, CDCl<sub>3</sub>) 8.29 (1H, s), 8.19 (2H, d, J 7.9), 8.17 (3H, d, J 7.9), 7.62–7.48 (4H, m), 7.41 (2H, t, J 7.6), 7.31 (2H, t, J 7.5), 7.07 (2H, d, J 8.1), 2.11 (3H, s). δ<sub>C</sub> (176 MHz, CDCl<sub>3</sub>) 164.9, 164.1, 140.8, 139.4, 138.5, 131.9, 130.12, 130.09, 129.1, 127.1, 126.1, 125.9, 124.1, 123.8, 123.1, 120.5, 120.1, 109.7, 17.5. MS (MALDI+): *m/z* 401.1 (M<sup>+</sup>, 100%).

2-[4-(9H-Carbazol-9-yl)-3-methylphenyl]-5-(2,4,6-trimethylphenyl)-1,3,4-oxadiazole (**5f**). Following the procedure for **5a**, **4f** (0.15 g, 0.5 mmol), carbazole (0.08 g, 0.9 mmol), K<sub>2</sub>CO<sub>3</sub> (200 mg), and DMSO (10 mL), with recrystallization of the product from acetonitrile gave **5f** (0.12 g, 45%) as colorless crystals. Mp: 191.3–192.6 °C. Anal. Calcd for C<sub>30</sub>H<sub>25</sub>N<sub>3</sub>O: C, 81.24; H, 5.68; N, 9.47. Found: C, 81.34; H, 5.73; N, 9.61. δ<sub>H</sub> (700 MHz, CDCl<sub>3</sub>) 8.25 (1H, s), 8.17 (2H, d, J 7.6), 8.13 (1H, d, J 10.1), 7.54 (1H, d, J 8.1), 7.41 (2H, t, J 7.6), 7.30 (2H, t, J 7.9), 7.06 (2H, d, J 8.1), 7.02 (2H, s), 2.37 (3H, s), 2.36 (6H, s), 2.09 (3H, s). δ<sub>C</sub> (176 MHz, CDCl<sub>3</sub>) 164.4, 164.3, 141.2, 140.7, 139.3, 138.7, 138.5, 130.1, 130.0, 128.9, 126.1, 125.8, 124.2, 123.3, 121.0, 120.5, 120.0, 109.6, 21.3, 20.5, 17.8. MS (MALDI+): *m/z* 443.2 (M<sup>+</sup>, 100%).

2-[4-(9H-Carbazol-9-yl)-3-methylphenyl]-5-(2,4,6-triisopropylphenyl)-1,3,4-oxadiazole (**5g**). Following the procedure for **5a**, **4g** (0.12 g, 0.31 mmol), carbazole (0.05 g, 0.31 mmol), K<sub>2</sub>CO<sub>3</sub> (200 mg), and DMSO (20 mL), with recrystallization of the product from acetonitrile, gave **5g** (0.10 g, 57%) as colorless crystals. Mp: 202.6–203.8 °C. Anal. Calcd for C<sub>36</sub>H<sub>37</sub>N<sub>3</sub>O: C, 81.94; H, 7.07; N, 7.96. Found: C, 81.80; H, 7.12; N, 8.07. δ<sub>H</sub> (700 MHz, CDCl<sub>3</sub>) 8.24 (1H, s), 8.16 (2H, d, J 7.8), 8.12 (1H, d, J 8.2), 7.54 (1H, d, J 8.1), 7.40 (2H, t, J 7.6), 7.30 (2H, t, J 7.8), 7.15 (2H, s), 7.06 (2H, d, J 8.1), 2.97 (1H, dt, J 6.9, 13.8), 2.70 (2H, dt, J 6.8, 13.5), 2.08 (3H, s), 1.30 (6H, t, J 9.1), 1.25 (12H, d, J 6.8). δ<sub>C</sub> (176 MHz, CDCl<sub>3</sub>) 164.6, 164.2, 152.5, 149.5, 140.7, 139.3, 138.6, 130.2, 130.0, 126.1, 125.8, 124.3, 123.3, 121.2, 120.5, 120.0, 119.6, 109.6, 34.6, 31.5, 24.1, 23.9, 17.8. MS (MALDI+): *m/z* 527.3 (M<sup>+</sup>, 100%). Crystals for X-ray analysis were grown by slowly cooling a solution of **5g** in MeCN.

-[4-(2,7-Dimethoxy-9H-carbazol-9-yl)phenyl]-5-(2,4,6-trimethylphenyl)-1,3,4-oxadiazole (**5h**). Following the procedure for **5a**, **4f** (0.07 g, 0.2 mmol), 2,7-dimethoxycarbazole (0.07 g, 0.3 mmol),  $K_2CO_3$  (200 mg), and DMSO (10 mL), with recrystallization of the product from acetonitrile, gave **5h** (0.05 g, 50%) as colorless crystals. Mp: 186.3–187.2 °C. Anal. Calcd for  $C_{32}H_{29}N_3O_3$ : C, 76.32; H, 5.80; N, 8.34. Found: C, 76.27; H, 5.85; N, 8.40.  $\delta_H$  (500 MHz,  $CDCl_3$ ) 8.28 (1H, s), 8.16 (1H, d, J 9.8), 7.94 (2H, d, J 8.5), 7.56 (1H, d, J 8.1), 7.05 (2H, s), 6.90 (2H, dd, J 3.3, 9.5), 6.49 (2H, d, J 2.2), 3.82 (6H, s), 2.40 (3H, s), 2.38 (6H, s), 2.14 (3H, s).  $\delta_C$  (126 MHz,  $CDCl_3$ ) 164.7, 164.5, 158.7, 142.4, 141.5, 139.4, 139.0, 138.9, 130.4, 129.2, 126.2, 124.6, 121.2, 120.6, 117.5, 108.6, 94.3, 55.9, 21.6, 20.8, 18.2. MS (ASAP+):  $m/z$  504.2 ( $M+H^+$ , 100%).

2-[4-(2,7-Dimethoxy-9H-carbazol-9-yl)phenyl]-5-(2,4,6-triisopropylphenyl)-1,3,4-oxadiazole (**5i**). Following the procedure for **5a**, **4c** (0.2 g, 0.5 mmol), 2,7-dimethoxycarbazole (0.2 g, 1.2 mmol),  $K_2CO_3$  (400 mg), and DMSO (20 mL), with recrystallization of the product from acetonitrile, gave **5i** (0.17 g, 60%) as colorless crystals. Mp: 192.5–194.0 °C. Anal. Calcd for  $C_{37}H_{39}N_3O_3$ : C, 77.46; H, 6.85; N, 7.32. Found: C, 77.35; H, 6.93; N, 7.35.  $\delta_H$  (500 MHz,  $CDCl_3$ ) 8.36 (2H, d, J 8.5), 7.93 (2H, d, J 9.2), 7.77 (2H, d, J 8.5), 7.18 (2H, s), 6.97–6.88 (4H, m), 3.86 (6H, s), 3.01 (1H, dt, J 7.0, 13.9), 2.79–2.67 (2H, m), 1.34 (6H, d, J 6.9), 1.28 (12H, d, J 6.8).  $\delta_C$  (126 MHz,  $CDCl_3$ ) 164.7, 164.4, 158.7, 152.8, 149.8, 142.0, 141.1, 128.9, 127.6, 123.1, 121.5, 120.6, 119.8, 118.0, 108.9, 94.6, 56.0, 34.9, 31.8, 24.4, 24.2. MS (ASAP+):  $m/z$  574.3 ( $M+H^+$ , 100%).

2-[4-(9H-Carbazol-9-yl)phenyl]-5-methyl-1,3,4-oxadiazole (**7a**). Following the procedure for **5a**, **6** (0.50 g, 2.8 mmol), carbazole (0.47 g, 2.8 mmol),  $K_2CO_3$  (1.9 g), and DMSO (40 mL) with elution of the product with dichloromethane followed by recrystallization from acetonitrile gave **7a** (0.55 g, 61%) as colorless crystals. Mp: 202.8–203.8 °C. Anal. Calcd for  $C_{21}H_{15}N_3O$ : C, 77.52; H, 4.65; N, 12.91. Found: C, 77.52; H, 4.67; N, 13.13.  $\delta_H$  (500 MHz,  $CDCl_3$ ) 8.30 (2H, d, J 8.6), 8.17 (2H, d, J 7.7), 7.77 (2H, d, J 8.6), 7.54–7.43 (4H, m), 7.34 (2H, t, J 7.4), 2.70 (3H, s).  $\delta_C$  (126 MHz,  $CDCl_3$ ) 164.6, 164.2, 141.0, 140.5, 128.6, 127.5, 126.5, 124.0, 122.8, 120.8, 120.7, 109.9, 11.5. MS (EI):  $m/z$  325.0 ( $M^+$ , 100%). Crystals for X-ray analysis were grown by slowly cooling a solution of **7a** in MeCN.

2-[4-(2,7-Dimethoxy-9H-carbazol-9-yl)phenyl]-5-methyl-1,3,4-oxadiazole (**7b**). Following the procedure for **7a**, **6** (0.24 g, 1.4 mmol), 2,7-dimethoxycarbazole (0.30 g, 1.4 mmol),  $K_2CO_3$  (800 mg), and DMSO (40 mL) gave **7b** (0.36 g, 73%) as colorless crystals. Mp: 226.9–228.3 °C. Anal. Calcd for  $C_{23}H_{19}N_3O_3$ : C, 71.67; H, 4.97; N, 10.90. Found: C, 71.27; H, 4.96; N, 10.81.  $\delta_H$  (700 MHz,  $CDCl_3$ ) 8.27 (2H, d, J 8.5), 7.89 (2H, d, J 8.4), 7.72 (2H, d, J 8.5), 6.91–6.86 (4H, m), 3.83 (6H, s), 2.67 (3H, s).  $\delta_C$  (176 MHz,  $CDCl_3$ ) 164.3, 163.8, 158.4, 141.7, 140.7, 128.5, 127.2, 122.7, 120.3, 117.7, 108.6, 94.4, 55.7, 11.2. MS (EI):  $m/z$  385.0 ( $M^+$ , 100%).

**Crystal Structure Determinations.** Single-crystal X-ray diffraction experiments (Table 3) were carried out using graphite-monochromated Mo  $K_\alpha$  radiation ( $\lambda = 0.71073$  Å) and open-flow  $N_2$  cryostats. The structures were solved by direct methods and refined by full-matrix least-squares on  $F^2$  of all data, using SHELXTL 6.14<sup>67</sup> and OLEX2 software.<sup>68</sup> Non-hydrogen atoms were refined with anisotropic displacement parameters, methyl groups as rigid bodies, and other H atoms as “riding” in idealized positions. In **5c**, the tri(isopropyl)phenyl fragment shows disorder which was resolved for four carbon atoms of the ring and two of the 4-isopropyl group, which were refined in two positions each with occupancies of 0.8 (anisotropic) and 0.2 (isotropic). Full crystallographic data, excluding structure factors, have been deposited at the Cambridge Crystallographic Data Center.

## ASSOCIATED CONTENT

**S Supporting Information.** X-ray crystal structures, NMR spectra, absorption and emission spectra, fluorescence decays,

cyclic voltammograms, and computational details. This material is available free of charge via the Internet at <http://pubs.acs.org>.

## AUTHOR INFORMATION

### Corresponding Author

\*E-mail: [m.r.bryce@durham.ac.uk](mailto:m.r.bryce@durham.ac.uk); [a.p.monkman@durham.ac.uk](mailto:a.p.monkman@durham.ac.uk).

## ACKNOWLEDGMENT

We thank the EPSRC for funding and John Dickinson for assistance with obtaining some of the photophysical data.

## REFERENCES

- (1) Albinsson, B.; Eng, M. P.; Pettersson, K.; Winters, M. U. *Phys. Chem. Chem. Phys.* **2007**, *9*, 5847–5864.
- (2) Fukuzumi, S.; Guldi, D. M. In *Electron Transfer in Chemistry*; Balzani, V., Ed.; Wiley-VCH: Weinheim, Germany; Vol. 2, pp 270–337.
- (3) Adams, D. M.; Brus, L.; Chidsey, C. E. D.; Greager, S.; Creutz, C.; Kagan, C. R.; Kamat, P. V.; Lieberman, M.; Lindsay, S.; Marcus, R. A.; Metzger, R. M.; Michel-Beyerle, M. E.; Miller, J. R.; Newton, M. D.; Rolison, D. R.; Sankey, O.; Schanze, K. S.; Yardley, J.; Zhu, X. *J. Phys. Chem. B* **2003**, *107*, 6668–6697.
- (4) Andrew, T. L.; Swager, T. M. *J. Polym. Sci., Part B: Polym. Phys.* **2011**, *49*, 476–498.
- (5) Special Issue:  $\pi$ -Functional Materials. *Chem. Mater.* **2011**, *23*, 309–922.
- (6) Maruccio, G.; R. Cingolani, R.; Rinaldi, R. *J. Mater. Chem.* **2004**, *14*, 542–554.
- (7) Troisi, A.; Ratner, M. A. *Small* **2006**, *2*, 172–181.
- (8) Special Issue: Organic Electronics. *Chem. Mater.* **2004**, *16*, 4381–4846.
- (9) Special Issue: Organic Electronics and Optoelectronics. *Chem. Rev.* **2007**, *107*, 923–1386.
- (10) Gust, D.; Moore, T. A.; Moore, A. L. *Acc. Chem. Res.* **2001**, *34*, 40–48.
- (11) *Organic Light-Emitting Devices*; Müllen, K., Scherf, U., Eds.; Wiley-VCH: Weinheim, 2006.
- (12) Review: Laquai, F.; Park, Y.-S.; Kim, J.-J.; Basché, T. *Macromol. Rapid Commun.* **2009**, *30*, 1203–1231.
- (13) Sun, Y.; Giebink, N. C.; Kanno, H.; Ma, B.; Thompson, M. E.; Forrest, S. R. *Nature* **2006**, *440*, 908–912.
- (14) Grimsdale, A. C.; Chan, K. L.; Martin, R. E.; Jokisz, P. G.; Holmes, A. B. *Chem. Rev.* **2009**, *109*, 897–1091.
- (15) Shirota, Y.; Kageyama, H. *Chem. Rev.* **2007**, *107*, 953–1010.
- (16) Delgado, J. L.; Bouit, P.-A.; Filippone, S.; Herranz, M. A.; Martín, N. *Chem. Commun.* **2010**, *46*, 4853–4865.
- (17) Giacalone, F.; Segura, J. L.; Martín, N.; Ramey, J.; Guldi, D. M. *Chem.—Eur. J.* **2005**, *11*, 4819–4834.
- (18) Thompson, A. L.; Ahn, T.-S.; Thomas, K. R. J.; Thayumanavan, S.; Martínez, T. J.; Bardeen, C. J. *J. Am. Chem. Soc.* **2005**, *127*, 16348–16349.
- (19) Adhikari, R. M.; Mondal, R.; Shah, B. K.; Neckers, D. C. *J. Org. Chem.* **2007**, *72*, 4727–4732.
- (20) Su, S.-J.; Sasabe, H.; Takeda, Kido, J. *Chem. Mater.* **2008**, *20*, 1691–1693.
- (21) Tao, Y.; Wang, Q.; Yang, C.; Zhong, C.; Zhang, K.; Qin, J.; Ma, D. *Adv. Funct. Mater.* **2010**, *20*, 304–311.
- (22) Tokito, S.; Iijima, T.; Suzuri, Y.; Kita, H.; Tsuzuki, T.; Sato, F. *Appl. Phys. Lett.* **2003**, *83*, 569–571.
- (23) Hanss, D.; Wenger, O. S. *Eur. J. Inorg. Chem.* **2009**, 3778–3790.
- (24) Schrögel, P.; Tomkevičienė, A.; Strohsriegel, P.; Hoffmann, S. T.; Köhler, A.; Lennartz, C. *J. Mater. Chem.* **2011**, *21*, 2266–2273.
- (25) Kamtekar, K. T.; Wang, C.; Bettington, S.; Batsanov, A. S.; Perepichka, I. F.; Bryce, M. R.; Ahn, J. H.; Rabinal, M.; Petty, M. C. *J. Mater. Chem.* **2006**, *16*, 3823–3835.

- (26) Hancock, J. M.; Gifford, A. P.; Zhu, Y.; Lou, Y.; Jenekhe, S. A. *Chem. Mater.* **2006**, *18*, 4924–4932.
- (27) Zhu, Y.; Kulkarni, A. P.; Wu, P.-T.; Jenekhe, S. A. *Chem. Mater.* **2008**, *20*, 4200–4211.
- (28) Kulkarni, A. P.; Zhu, Y.; Babel, A.; Wu, P. T.; Jenekhe, S. A. *Chem. Mater.* **2008**, *20*, 4212–4223.
- (29) Takizawa, S.; Montes, V. A.; Anzenbacher, P., Jr. *Chem. Mater.* **2009**, *21*, 2452–2458.
- (30) Zeng, L. C.; Lee, T. Y. H.; Merkel, P. B.; Chen, S. H. *J. Mater. Chem.* **2009**, *19*, 8772–8781.
- (31) Estrada, L. A.; Neckers, D. C. *J. Org. Chem.* **2009**, *74*, 8484–8487.
- (32) Gong, S. L.; Zhao, Y. B. A.; Yang, C. L.; Zhong, C.; Qin, J. G.; Ma, D. G. *J. Phys. Chem. C* **2009**, *114*, 5193–5198.
- (33) Duan, L.; Qiao, J.; Sun, Y.; Qiu, Y. *Adv. Mater.* **2011**, *23*, 1137–1144.
- (34) Chaskar, A.; Chen, H.-F.; Wong, K.-T. *Adv. Mater.* **2011**, *23*, 3876–3895.
- (35) van Dijken, A.; Bastiaansen, J. J. A. M.; Kiggen, N. M. M.; Langeveld, B. M. W.; Rothe, C.; Monkman, A.; Bach, I.; Stössel, P.; Brunner, K. *J. Am. Chem. Soc.* **2004**, *126*, 7718–7727.
- (36) Boudreaault, P.-L. T.; Beaupré, S.; Leclerc, M. *Polym. Chem.* **2010**, *1*, 127–136.
- (37) Lo, S.-C.; Burn, P. L. *Chem. Rev.* **2007**, *107*, 1097–1116.
- (38) Abia, A. A.; Burkhart, R. D. *Macromolecules* **1984**, *17*, 2739–2744.
- (39) O'Brien, D. F.; Baldo, M. A.; Thompson, M. E.; Forrest, S. R. *Appl. Phys. Lett.* **1999**, *74*, 442–444.
- (40) Adamovich, V.; Brooks, J.; Tamayo, A.; Alexander, A. M.; Djurovich, P. I.; D'Andrade, B. W.; Adachi, C.; Forrest, S. R.; Thompson, M. E. *New J. Chem.* **2002**, *26*, 1171–1178.
- (41) Chien, C.-H.; Hsu, F.-M.; Shu, C.-F.; Chi, Y. *Org. Electron.* **2009**, *10*, 871–876.
- (42) Muneuchi, K.; Sasaki, M.; Sasabe, H.; Adachi, C. *Jpn. J. Appl. Phys.* **2010**, *49*, 080208.
- (43) Jankus, V.; Winscom, C.; Monkman, A. P. *J. Chem. Phys.* **2009**, *130*, 074501.
- (44) Review: Kulkarni, A. P.; Tonzola, C. J.; Babel, A.; Jenekhe, S. A. *Chem. Mater.* **2004**, *16*, 4556–4573.
- (45) Review: Hughes, G.; Bryce, M. R. *J. Mater. Chem.* **2005**, *15*, 94–107.
- (46) *Highly Efficient OLEDs with Phosphorescent Materials*; Yersin, H., Ed.; Wiley-VCH Verlag GmbH & Co. KGaA: Weinheim, 2008; Chapter 8, p 290.
- (47) Thomas, K. R. J.; Linn, J. T.; Tao, Y.-T.; Chuen, C.-H. *Chem. Mater.* **2004**, *16*, 5437–5444.
- (48) Guan, M.; Bian, Z. Q.; Zhou, Y. F.; Li, F. Y.; Li, Z. J.; Huang, C. H. *Chem. Commun.* **2003**, 2708–2709.
- (49) Tao, Y.; Wang, Q.; Yang, C.; Wang, Q.; Zhang, Z.; Zou, T.; Qin, J.; Ma, D. *Angew. Chem.* **2008**, *120*, 8224–8227.
- (50) Tao, Y. T.; Wang, Q.; Yang, C. L.; Zhong, C.; Zhang, K.; Qin, J. G.; Ma, D. G. *Adv. Funct. Mater.* **2010**, *20*, 304–311.
- (51) Sauer, J.; Huisgen, R.; Sturm, H. *J. Tetrahedron* **1960**, *11*, 241–251.
- (52) Kothari, P. J.; Singh, S. P.; Parmar, S. S.; Stenberg, V. I. *J. Heterocycl. Chem.* **1980**, *17*, 1393–1398.
- (53) Koyama, M.; Ohtani, N.; Kai, F.; Moriguchi, I.; Inouye, S. *J. Med. Chem.* **1987**, *30*, 552–562.
- (54) Barrett, D. G.; Boncek, V. M.; Catalano, J. G.; Deaton, D. N.; Hassell, A. M.; Jurgensen, C. H.; Long, S. T.; McFadyen, R. B.; Miller, A. B.; Miller, L. R.; Payne, J. A.; Ray, J. A.; Samano, V.; Shewchuk, L. M.; Tavares, F. X.; Wells-Knecht, K. J.; Willard, D. H., Jr.; Wright, L. L.; Zhou, H.-Q. *Bioorg. Med. Chem. Lett.* **2005**, *15*, 3540–3546.
- (55) Allen, F. H.; Taylor, R. *Chem. Soc. Rev.* **2004**, *33*, 463–475.
- (56) Dias, F. B.; Pollock, S.; Hedley, G.; Pålsson, L.-O.; Monkman, A. P.; Perepichka, I. I.; Perepichka, I. F.; Tavasli, M.; Bryce, M. R. *J. Phys. Chem. B* **2006**, *110*, 19329–19339.
- (57) Dias, F. B.; King, S.; Monkman, A. P.; Perepichka, I. I.; Kryuchkov, M. A.; Perepichka, I. F.; Bryce, M. R. *J. Phys. Chem. B* **2008**, *112*, 6557–6566.
- (58) Sinha, S.; Rothe, C.; Guntner, R.; Scherf, U.; Monkman, A. P. *Phys. Rev. Lett.* **2003**, *90*, 127402.
- (59) Jankus, V.; Winscom, C.; Monkman, A. P. *J. Phys. Condens. Matter* **2010**, *22*, 185802.
- (60) Pope, M.; Swenberg, C. E. *Electronic Processes in Organic Crystals*; Oxford University Press: New York, 1982; Chapter I.C.6, p 32.
- (61) Brunner, K.; van Dijken, A.; Börner, H.; Bastiaansen, J. J. A. M.; Kiggen, N. M. M.; Langeveld, B. M. W. *J. Am. Chem. Soc.* **2004**, *126*, 6035–6042.
- (62) Tao, Y.; Gong, S.; Wang, Q.; Zhong, C.; Yang, C.; Qin, J.; Ma, D. *Phys. Chem. Chem. Phys.* **2010**, *12*, 2438–2442.
- (63) Admassie, S.; Inganäs, O.; Mammo, W.; Perzon, E.; Andersson, M. R. *Synth. Met.* **2006**, *156*, 614–623.
- (64) Rothe, C.; Monkman, A. P. *Phys. Rev. B* **2003**, *68*, 075208.
- (65) Milcent, R.; Barbier, G. *J. Heterocycl. Chem.* **1983**, *20*, 77–80.
- (66) Zheng, Y.; Batsanov, A. S.; Bryce, M. R. *Inorg. Chem.* **2011**, *50*, 3354–3362.
- (67) Sheldrick, G. M. *Acta Crystallogr.* **2008**, *A64*, 112–122.
- (68) Dolomanov, O. V.; Bourhis, L. J.; Gildea, R. J.; Howard, J. A. K.; Puschmann, H. *J. Appl. Crystallogr.* **2009**, *42*, 339–341.